LANGMUIR

pubs.acs.org/Langmuir Article

In Vitro and Ex Planta Gold-Bonded and Gold-Mineralized Tobacco Mosaic Virus

Yifeng Ma, Zhuohong Wu, and Nicole F. Steinmetz*



Cite This: Langmuir 2023, 39, 11238-11244



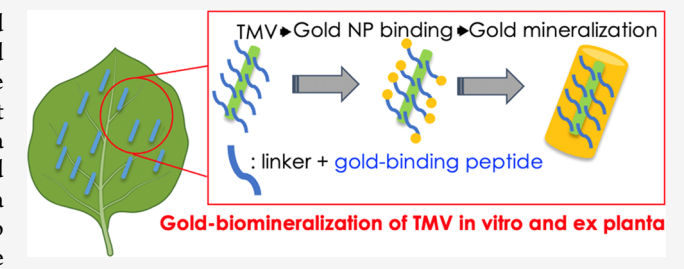
ACCESS

Metrics & More

Article Recommendations

Supporting Information

ABSTRACT: Biotemplated mineralization is a promising and ecofriendly approach to manufacture metal nanoparticles and composites with precise size control. Plant viruses are suitable templates for biomineralization because they are chemically robust and highly scalable through molecular farming. Here, we report a gold-nanoparticle-coated tobacco mosaic virus (TMV) synthesized in a test tube or in plant extracts making use of a TMV displaying a gold-binding peptide (GBP). The methods developed are a step toward engineered living materials, where gold nanowires could be formed in plant tissues for sensing or energy harvest applications.



INTRODUCTION

Nanoparticles offer a wide range of applications spanning the biomedical, agricultural, and energy storage fields. High-aspect-ratio gold nanorods have gained significant attention based on their unique physicochemical properties. In particular, metallic or metal-containing gold nanorods have unique optical properties. The scattering plasmon band of a gold nanorod falls in the near-infrared region of the light spectrum³ and can be tailored by altering the size and shape of the nanorods. This enhanced electromagnetic plasmonic system makes gold nanorods promising candidates as label-free sensors, herapeutic agents (i.e., cancer photothermal therapy, immunotherapy), molecular imaging probes, photocatalysts, and fuel cell materials.

While the development pipeline of gold nanorods is rapidly expanding, there is a need for the development of advanced fabrication techniques. The most common synthesis routes use electromagnetic irradiation, ¹⁰ chemical reduction, ¹¹ and topto-bottom fabrication methods such as laser ablation, ¹² thermal evaporation, ¹³ and lithography. ¹⁴ While highly sophisticated, these techniques have drawbacks, as they are expensive and time-consuming, require hazardous reaction conditions, and often yield toxic byproducts. The development of approaches yielding gold nanorods following the green chemistry principle, i.e., synthesis with maximized yield while minimizing toxicity and pollution, is an important goal in materials chemistry. An approach toward this goal is found in biotemplating or biomineralization and an intriguing template material with high-aspect-ratio soft matter nanorods formed by plant viruses and bacteriophages. ^{15–17}

To date, biotemplating approaches have focused on test tube reactions using purified viral nanoparticles. However, recent studies have reported that metallic nanoparticles can be produced using plant extracts. Bioactive compounds, such as polyphenols, terpenes, organic acids, and enzymes, serve as reductants within the plant extracts to reduce and stabilize gold nanoparticles from precursor salts. Gold nanoparticles of distinct shapes, although mostly of spherical and triangular shape, have been reported making use of various plant bioactive molecules from different plant species. 19

Here, we sought to investigate whether the high-aspect-ratio nanorods from the tobacco mosaic virus (TMV) could serve as a template for gold nanoparticle synthesis in plants. The establishment of these techniques would yield a route toward the biosynthesis of metallic nanoparticles in plants, either for harvest, purification, and use or the *in planta* synthesis of gold nanowires may allow the production of conducting and/or sensing elements to interface plants with technology. For example, the use of carbon nanotubes as sensor devices in living spinach plants was reported;²⁰ however, here, the nanoparticles have to be manually infiltrated, which may make in-field applications an unattainable option. The use of plant viruses and the expression of virus-like particles in plants may be a platform for engineered living plants enhanced with electronic components.

As proof of concept, we demonstrate biotemplating of TMV in plant extracts. TMV is a 300 nm \times 18 nm rod-shaped plant virus. ²¹ It is composed of 2130 identical coat proteins with a single-stranded, positive-sense RNA embedded into the protein scaffold. ²² For this work, we made use of native

Received: March 13, 2023 Revised: July 25, 2023 Published: August 4, 2023





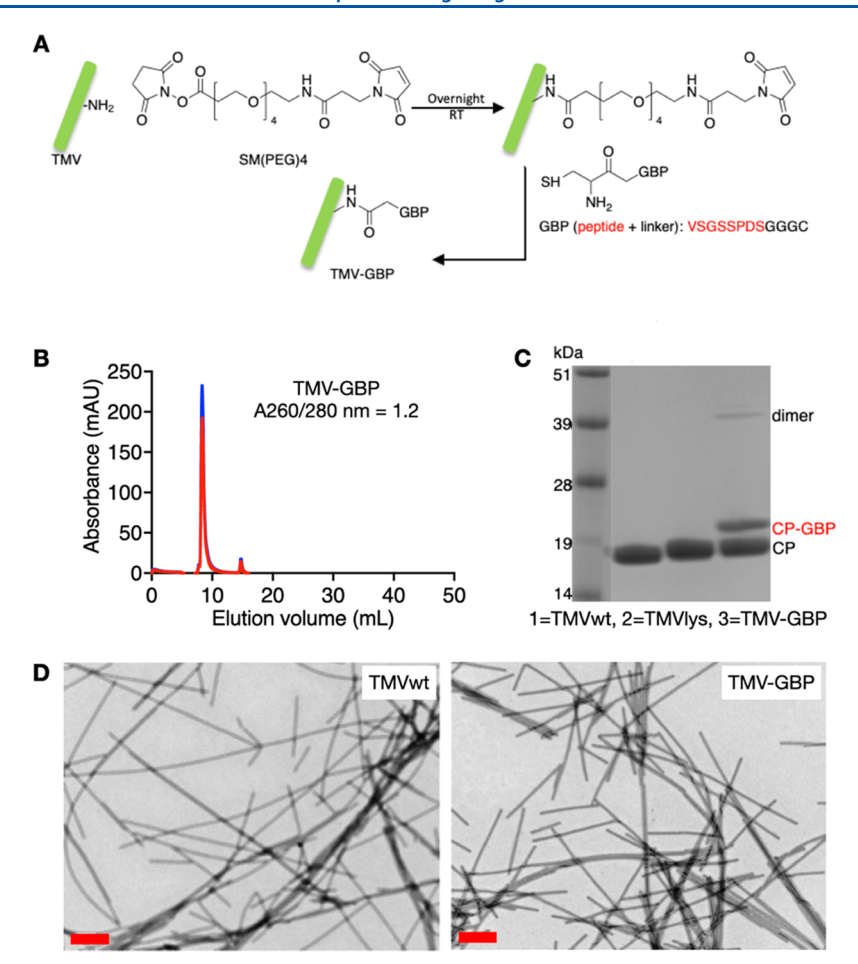


Figure 1. Chemical conjugation of a gold-binding peptide (GBP) to TMV and characterization of TMV-GBP. (A) Synthesis scheme to obtain TMV-GBP. (B) Size exclusion chromatography (SEC) of TMV-GBP showing the typical elution profile of intact TMV. (c) SDS-PAGE of wild-type TMV (TMVwt), lysine-added TMV (TMVlys), and TMV-GBP displaying the GBP. (d) TEM image of negatively stained TMVwt and TMV-GBP (scale bar: 400 nm).

TMV (TMVwt), a lysine-added mutant of TMV, termed TMVLys, ²³ and a gold-binding-peptide (GBP)-modified TMV, termed TMV-GBP. The lysine group equipped on every coat protein provides chemical addressability; we used a cysteine-terminated GBP for conjugation to the lysine side chains via a bifunctional *N*-hydroxysuccinimide (NHS)–PEG₄–maleimide (SM-PEG₄) linker (SM-PEG₄). First, we verified gold binding to TMV-GBP, either by binding TMV-GBP to gold surfaces or binding gold nanoparticles to TMV-GBP. Then, we demonstrated the test tube and ex planta mineralization to TMV-GBP. The resulting composite material, Au-TMV-GBP, was characterized using a combination of spectroscopy and microscopy techniques.

■ RESULTS AND DISCUSSION

The synthesis scheme of gold-binding TMV (TMV-GBP) is shown in Figure 1A. The solvent-exposed lysine groups on the TMV lysine (TMVlys) variant were first modified with a bifunctional SM-PEG₄ linker. The maleimide group was then further reacted with the cysteine-terminated GBP peptide, VSGSSPDSGGGC (MW = 1008.03 Da; the cysteine-reactive group was added via a GGG spacer). The discovery and application of the GBP peptide have been reported elsewhere. 24

Post-synthesis, size exclusion chromatography (SEC) and transmission electron microscopy (TEM) were used to

examine the structural integrity of TMV-GBP. The elution profile from the Superose 6 Increase column was consistent with intact TMV being released from the column at an 8 mL volume (Figures 1A and S1); the A260-to-A280 ratio of 1.2 is also consistent with intact TMV-GBP being produced. The secondary peak at 15 mL is indicative of free coat protein or particle breakage but only makes upto ~5% of the nanoparticle preparation. This peak is also apparent in the starting material with ~10% broken TMVlys particles observed by SEC. Thus, data indicate that the conjugation reaction does not affect the particle integrity. TEM imaging (Figure 1D) was in agreement with SEC data showing the typical high-aspect-ratio nanorods of TMV; there were no differences comparing TMV vs TMV-GBP. The appearance of longer rods (>300 nm) may be due to drying processes; there is a tendency for TMV particles to align end-to-end.

To verify the covalent attachment of the GBP peptide to TMV, we characterized TMV coat proteins using denaturing gel electrophoresis (SDS-PAGE, Figure 1C). The coat protein band was detected for all TMV formulations (at \sim 18 kDa); for TMV-GBP, an additional, higher-molecular-weight band appeared at \sim 20 kDa, which is consistent with the weight increase from GBP conjugation. Band analysis using ImageJ software indicates that \sim 33% of the coat proteins were conjugated with the GBP peptide. A coat protein dimer was also apparent on SDS-PAGE for the TMV-GBP formulation

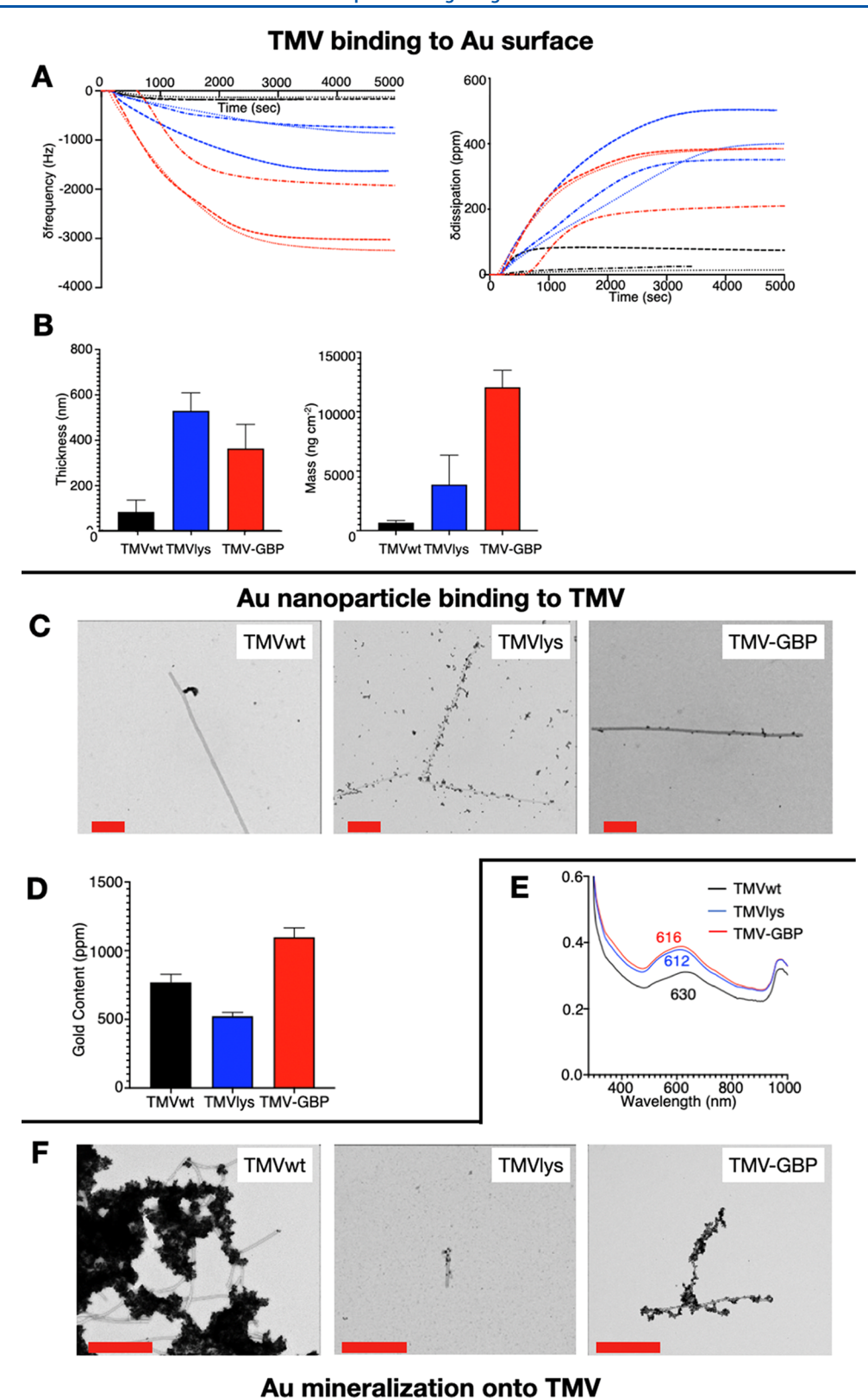


Figure 2. TMV-GBP gold affinity and reduction. TMV binding to gold surfaces (A, B). Gold nanoparticle binding to TMV (C, D) and gold mineralization was tested. (A) QCM-D analysis of TMVwt (black), TMVlys (blue), and TMV-GBP (red) binding to a gold-coated sensor (n = 3); (left) change in frequency and (right) dissipation shift for the third overtone of the resonance frequency in each experiment are shown with different dashed patterns. (B) Layer thickness was calculated with Sauerbrey's equation and mass calculated was calculated using a viscoelastic model, the Voigt model. (C) Immunocapture TEM of TMVwt, TMVlys, and TMV-GBP upon interaction with 5 nm gold nanoparticles (scale bar: 200 nm). (D) ICP-MS of the precipitant from the gold nanoparticle binding test using TMVwt, TMVlys, and TMV-GBP (n = 5). (E, F) Two-step biomineralization by the gold nanoparticle seeding followed by gold reduction from precursor salts onto TMVwt, TMVlys, or TMV-GBP. (E) Absorbance scan and (F) immunocapture TEM (scale bar: 500 nm).

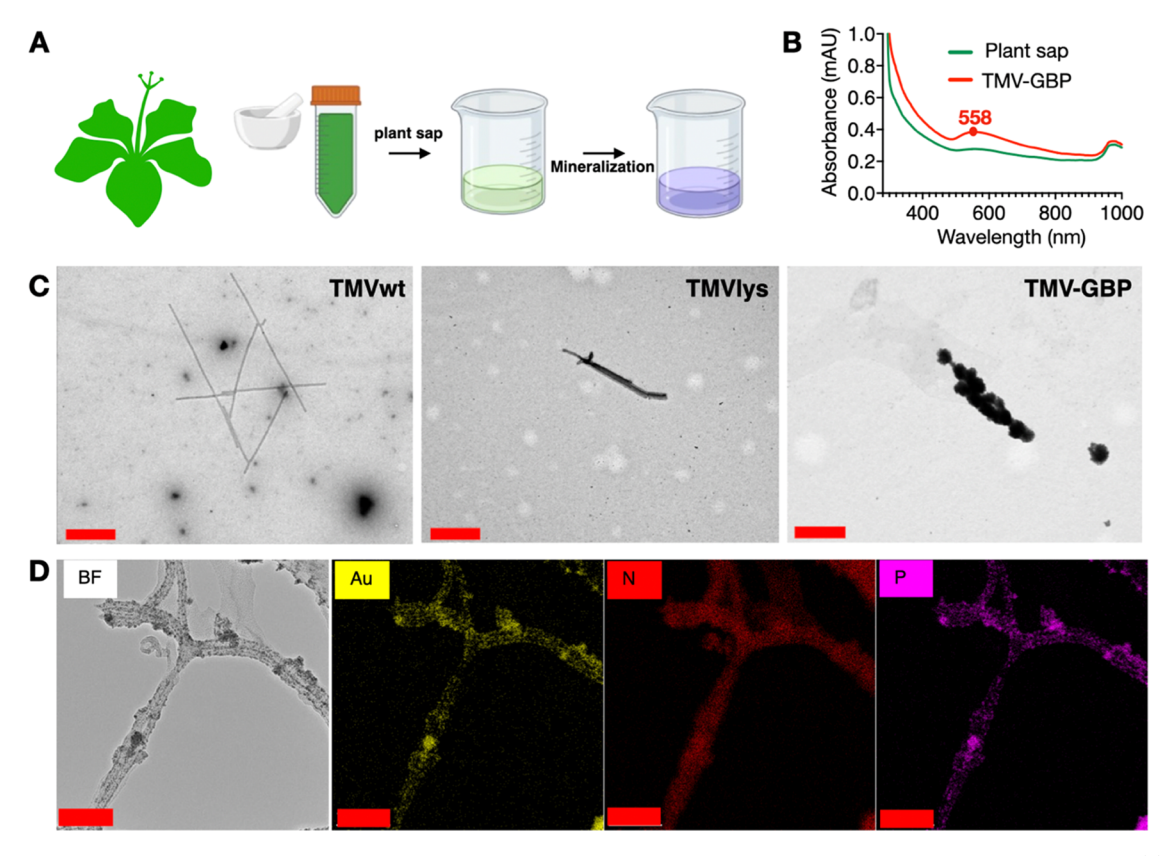


Figure 3. Spectral, morphological, and elemental characterization of TMV-GBP post-mineralization in *N. benthamiana* leaf extracts. (a) *Ex planta* mineralization scheme, (b) UV—vis absorbance spectra of gold-mineralized TMV-GBP (mineralization was at a 0.8 mg/mL protein concentration), and (c) TEM images of TMVwt, TMVlys, and TMV-GBP (at 0.1 m/mL) after gold mineralization in plant extracts (through the addition of chloroauric acid; scale bar: 200 nm). (d). Bright-field (BF) and EDX mapping of Au, N, and P using TMV-GBP post *ex planta* gold mineralization (scale bar: 100 nm; at 0.8 mg/mL).

(<4%); this is frequently observed for chemically modified TMV²¹ and explained by possible entanglement of the peptide-modified coat proteins.

With TMV-GBP in hand, we tested its properties to bind to gold surfaces, bind gold nanoparticles, and serve as a template for biomineralization. First, TMV vs TMV-GBP binding to gold surfaces was monitored using a quartz crystal microbalance with dissipation monitoring (QCM-D) using goldcoated sensors. QCM-D measures mass changes in real-time at nanoscale resolution by measuring the resonance frequency created by the alternating voltage; changes in dissipation (energy loss) provide insights into the viscoelastic properties.²⁵ Based on QCM-D (Figures 2A,B and S2), TMV-GBP absorption onto the gold surface yields a 2730 \pm 708 Hz shift, which is more prominent than 159 ± 24 and 1077 ± 481 Hz shifts measured for TMVwt and TMVlys. The mass of the deposited material was calculated using the Voigt model, a viscoelastic model that is appropriate to use when energy loss in the system is high (large changes in dissipation). The thickness of the virus layer, however, was calculated using Sauerbrey's equation to exclude mass from water molecules trapped within the hydrophilic virus particles; this analysis is consistent with prior QCM-D studies using plant virus assemblies.²⁷ Using this analysis, 12,045 ± 1434 ng cm⁻² TMV-GBP was absorbed on the gold sensor surface, forming a 363 ± 106 nm thickness, whereas 664 ± 185 ng cm⁻² TMVwt $(84 \pm 52 \text{ nm}) \text{ and } 3875 \pm 2459 \text{ ng cm}^{-2} \text{ TMVlys } (530 \pm 79 \text{ mg/s})$ nm) were deposited. QCM-D indicates that TMVwt and TMVlys were nonspecifically absorbed on the metallic

surface—this is consistent with previous reports and may be explained by gold—protein interactions through solvent-exposed carboxylic acid and hydroxyl groups.^{28,29} The increased binding of TMVlys vs TMVwt may be explained by the altered surface charge as a result of the lysine corona or a weak covalent and van der Waals interactions³⁰ between the nitrogen of the lysine residue and the gold substrate. It is worth noting that TMVlys deposition results in larger thickness albeit smaller mass change compared to TMV-GBP. In other words, the frequency change for TMVlys is small but accompanied by a large dissipation change, indicating that less material is more loosely bound. This is in stark contrast to TMGV-GBP and indicates that the engineered gold-binding TMV-GBP indeed has a stronger affinity to the gold substrate as a function of the

Second, we assayed the efficiency of 5 nm gold nanoparticles to bind to TMVwt, TMVlys, and TMV-GBP. A gold nanoparticle solution was prepared by adding 10% by volume 1 M NaCl solution in 10 mM PBS to 5-nm-sized gold nanoparticles (OD = 1 in 10 mM PBS). The gold nanoparticles were then mixed with TMVwt, TMVlys, and TMV-GBP (500:1) for 10 min at room temperature. TEM imaging (Figure 2C) was then performed analyzing the reaction mixture. Immunocapture was performed by using TEM grid-coated anti-TMV antibodies. Imaging confirmed that indeed gold nanoparticles were bound to TMV-GBP. It was interesting to note that by TEM, the TMVlys appeared to be the most efficient gold nanoparticle binder. To gain quantitative insights and rule out unstable gold binding, gold

nanoparticle-bonded TMV samples (TMVwt, TMVlys, TMV-GBP) were purified by centrifugation and subjected to ICP-MS analysis (Figure 2D). Increased Au content was detected for TMV-GBP: with 1097.0 \pm 69.2 ppm Au for TMV-GBP compared to 769.6 \pm 59.4 ppm Au for TMVwt and 521.4 \pm 28.4 ppm Au for TMVlys. Thus, we conclude that TMV-GBP serves as a scaffold to bind gold nanoparticles from the solution. While TMVlys also appears to be a gold binder, the interactions may be weaker and less specific.

Third, we subjected TMV-GBP to a biomineralization experiment to assay whether TMV-GBP can catalyze the reduction of precursor salts to yield gold nanoparticles. Here, a two-step procedure was done: first, we seeded 5 nm gold nanoparticles onto the TMV nanoparticles, and second, chloroauric acid was then added to be reduced and increase the gold nanoparticle coverage.³¹ Optical absorbance scans (Figure 2E) and TEM images (Figure 2F, again immunocapture TEM was performed) highlight significant differences between the gold reduction of gold-seeded TMVwt, TMVlys, and TMV-GBP. While the mineralization conditions largely induced aggregation of TMVwt, coatings with gold nanoparticles of varying sizes were observed for TMV-GBP, with a higher coating density compared to TMVlys. The optical properties of gold nanorods are a function of the gold nanoshell thickness.³² Also, the gold colloidal size and shape determine the shape of the absorbance spectrum.³³ Therefore, optical absorbance scans were performed within the wavelength range of 230-1000 nm (Figure 2E). As evident from TEM, gold was present in all samples, but the peak profiles differed: The absorbance peaks for gold-coated TMV-GBP and TMVlys were 616 and 612 nm, respectively, while gold-coated TMVwt exhibited a right-shifted absorbance peak at 630 nm, which may be a result of the high degree of aggregation as observed by TEM.³⁴

Further, the sharpest peak was observed for TMV-GBP; this sample exhibited a peak width of <220 nm, while the peaks for TMVlys and TMVwt measured 247 and 259 nm, respectively. These data indicate the formation of gold-binding products in all three experimental groups.

Lastly, with the long-term goal of in planta generation of gold nanowires, we investigated here whether the gold-binding and mineralization properties could be accomplished in plant extracts (Figure 3). Nicotiana benthamiana leaves were chosen because tobacco is a host of TMV.²³ Leaf extracts were obtained and spiked with TMVwt, TMVlys, or TMV-GBP; then, biomineralization was carried out through the addition of chloroauric acid (Figure 3A). Spectral analysis indicates successful gold biomineralization using TMV-GBP, as evident by the characteristic 558 nm absorbance peak (Figure 3B). Spectral data were corroborated by TEM imaging, which also confirmed that gold nanoclusters were deposited on the TMV-GBP template (Figure 3C). Biomineralization of TMV and TMVlys was not apparent, therefore confirming the goldbinding function conferred by the peptide added to TMV-GBP. These data are consistent with the test tube experiment data previously reported with purified viral nanoparticles in buffer and indicate TMV-GBP to be a suitable template for gold nanowire synthesis. Lastly, we performed elemental analysis using EDX mapping: bright-field (BF) TEM images and energy-dispersive X-ray (EDX) elemental mapping are shown in Figure 3D, and the analysis confirmed the colocalization of nitrogen (N) and phosphate (P) elements

from TMV and gold (Au) elements from the newly synthesized gold nanoparticles.

CONCLUSIONS

We developed TMV-GBP nanoparticles with affinity to gold surfaces and gold nanoparticles suitable for gold biomineralization. In particular, we demonstrated that TMV-GBP may be a suitable material, enabling the formation of gold nanowires in complex media, such as leaf extracts. Future goals are to perform synthesis of such hybrid materials *in planta*, which may lead to engineered living plants enhanced by synthetic elements. On the other hand, harvesting plasmonic materials directly from plants could be feasible. The developed approach might also be adapted for metal mineralization other than gold to evolve more properties.

■ EXPERIMENTAL SECTION

Gold-Binding Peptide (GBP) Conjugation to TMV. TMV and its lysine variant (TMVlys) were propagated in and isolated from Nicotiana benthamiana plants following established protocols.²³ GBP (VSGSSPDSGGGC) was synthesized and obtained from GenScript. For GBP conjugation, TMVlys was first functionalized with bifunctional linker SM(PEG)₄. Specifically, for every 1 mL reaction, a 5-fold excess of SM(PEG)₄ per coat protein was reacted with 2 mg of TMVlys in 10 mM potassium phosphate (KP) buffer (pH 7.4) with 10% (v/v) dimethyl sulfoxide (DMSO) for 2 h at room temperature on an orbital shaker. Excess linker was removed from TMV-(PEG)₄-maleimide by ultracentrifugation at 120,000g for 1 h at 4 °C over 0.2 mL of 40% (w/v) sucrose cushion. TMV-(PEG)₄maleimide was resuspended in a 10 mM KP buffer (pH 7.4). GBP was then added at a 2-fold excess per coat protein to TMV-(PEG)₄maleimide (2 mg mL⁻¹), and the reaction was allowed to proceed overnight at room temperature on an orbital shaker. The resulting TMV-GBP was purified from the reaction mixture by ultracentrifugation at 120,000g for 1 h at 4 °C, resuspended, and stored in 10 mM KP buffer (pH 7.4).

Quartz Crystal Microbalance with Dissipation Monitoring (QCM-D). TMV gold binding was monitored by a QCM-D using gold-coated chips. A gold-coated QSense sensor (Biolin Scientific) was cleaned by UV/ozone treatment for 10 min, incubated in 25% aqueous ammonia and a 30% hydrogen peroxide solution for 5 min at 75 °C, followed by another 10 min UV/ozone treatment, and dried completely under a nitrogen flow. The flow module (Qsense, Biolin Scientific) and the tubing were cleaned with a 2% (w/v) SDS solution and Millipore water for 10 min with a 300 μ L min⁻¹ flow rate. Then, 0.2 mg mL⁻² TMV samples in 10 mM KP buffer were added at a 20 μ L min⁻¹ flow rate until the change in frequency and energy loss profile plateau. The profile was analyzed with Dfind software (Biolin Scientific).

Gold-Binding Test. Further, 6.204 mg mL $^{-1}$ TMV samples (6.204 mg mL $^{-1}$) were incubated in 1 mL of 5 nm gold nanoparticles (Thermo Scientific, OD 1 in 0.1 mM PBS) with 10% volume 1 M NaCl added for 10 min at room temperature.

Gold Nanoparticle Seeding and Biomineralization. A gold biomineralization synthesis protocol was adapted from the literature. Specifically, in a 1 mL reaction, 1.2×10^{11} TMV particles were first seeded with 5 nm gold nanoparticles (1:40,000) in 10 mM KP buffer (pH 7.4). Then, 99.69 μ L of 1 M NaCl was added to increase the ionic strength of the solution. After incubating the reaction mixture at room temperature for 20 min, 13 μ L of a 0.4 mM HAuCl₄ + 1.8 mM K₂CO₃ mixture was added with 20 μ L of 18 mM HONH₂·HCl, vortexed quickly, and incubated for 5 min. The samples were characterized right away post-synthesis.

Ex Planta Gold Biomineralization of TMV. The plant sap was obtained from *N. benthamiana* leaves, and TMVwt, TMVlys, or TMV-GBP was spiked into the plant sap at a 0.1 or 0.8 mg/mL protein concentration, and then 1 mM HAuCl₄ in 50 mM PBS buffer (pH

5.0) was added followed by incubation at 37 $^{\circ}$ C for 48 h. Mineralized TMV samples were then analyzed by TEM and UV—vis spectrometry.

UV–Vis Spectrometry. The concentration of TMVwt, TMVlys, and TMV-GBP was measured with a NanoDrop 2000 spectrophotometer and calculated with the extinction coefficient 3.0 mL mg $^{-1}$ cm $^{-1}$ at 260 nm. 21 Absorption spectra were recorded with 200 μ L of the sample in a Nunc MicroWellTM 96-well microplate (Thermo Fisher) using an Infinite M200 plate reader (Tecan) and plotted with GraphPad Prism 9.

Sodium Dodecyl Sulfate-Polyacrylamide Gel Electrophoresis (SDS-PAGE). Ten microliters of native and or GBP-conjugated TMV (1 mg mL⁻¹) were heated at 100 °C for 5 min with NuPAGE LDS sample buffer (4×) (Invitrogen, Thermo Fisher Scientific) and loaded into the wells. The samples were run along with the SeeBlue Plus2 prestained protein standard ladder (Invitrogen, Thermo Fisher Scientific) in 3-(morpholin-4-yl)propane-1-sulfonic acid (MOPS) buffer (Thermo Fisher Scientific) at 200 V for 40 min. The gel was first immersed in a destaining solution composed of 10% acetic acid and 50% methanol in DI water for 1 h to avoid oversaturated staining. The gel was then stained with 0.25% Coomassie Brilliant Blue R-250 (Fisher BioReagents) and imaged using a FluorChem R imaging system (ProteinSimple). Band analysis was performed using Fiji Image] software (https://imagej.net/software/fiji/).

Fast Protein Liquid Chromatography (FPLC). Two hundred microliters of 3 mg mL⁻¹ TMV in 10 mM KP buffer (pH 7.4) were loaded onto a KTA pure 25 M1 (Cytiva) equipped with a Superose 6 Increase column (Cytiva). The flow rate was set at 0.5 mg mL⁻¹. The absorbance at 260 and 280 nm was measured.

Transmission Electron Microscopy. For immunocapture TEM, TMV affinity grids were prepared as reported in the literature.³⁵ Briefly, a Formvar/carbon film grid (Electron Microscopy Sciences) was glow discharged with 15 mA current for 30 s under 0.15 mbar in a PELCO easiGlow glow discharge cleaning system (TED PELLA, INC.). Three microliters of 10 µg mL⁻¹ rabbit anti-TMV antibody (Agdia) were added onto the carbon side of the glow-discharged grid and incubated for 3 min. Ten microliters of TMV samples were then loaded onto the grid as follows: 10 µL of TMV, TMVlys, and TMV-GBP (0.5 mg mL⁻¹) with or without gold were incubated on the grid for 2 min at room temperature. The grids were then washed twice using 10 μ L of water (30 s each time) and then stained twice using 10 μ L of 2% (w/v) uranyl acetate (45 s each time). The grid was blotted dry and imaged with a Gatan OneView camera (Bluescientific) equipped with a JEOL 1400 plus transmission electron microscope at 80 kV; images were captured using a Gatan 4k digital camera. Electron dispersive X-ray spectroscopy (EDX) images were obtained using a Thermo Fisher Talos 200X operating at 200 kV. Scanning TEM images and energy-dispersive spectrometry (EDS) mapping were performed by using Thermo Scientific software.

Inductively Coupled Plasma-Mass Spectroscopy (ICP-MS). The gold concentration was measured with ICP-MS. The reaction product from the gold-binding test was centrifuged at 14,478g (Microfuge 16, Beckman Coulter) for 2 min. The precipitant and last 15 μ L of the liquid were kept for ICP-MS sample preparation: 5 mL of 2% v/v nitric acid was added and heated at 95 °C for 10 min. Further, 1, 10, 100, and 1000 ppb gold standards were prepared with TraceCERT Gold Standard for ICP (Millipore Sigma) and 2% v/v nitric acid. The sample was measured with a Thermo iCAP RQ ICP-MS.

ASSOCIATED CONTENT

5 Supporting Information

The Supporting Information is available free of charge at https://pubs.acs.org/doi/10.1021/acs.langmuir.3c00688.

Additional SEC and QCM-D data plots (PDF)

AUTHOR INFORMATION

Corresponding Author

Nicole F. Steinmetz — Department of NanoEngineering, University of California, San Diego, La Jolla, California 92039, United States; Department of Bioengineering, Department of Radiology, Center for Nano-ImmunoEngineering, Moores Cancer Center, and Institute for Materials Discovery and Design, University of California, San Diego, La Jolla, California 92039, United States; orcid.org/0000-0002-0130-0481; Email: nsteinmetz@ucsd.edu

Authors

Yifeng Ma — Department of NanoEngineering, University of California, San Diego, La Jolla, California 92039, United States

Zhuohong Wu – Department of NanoEngineering, University of California, San Diego, La Jolla, California 92039, United States

Complete contact information is available at: https://pubs.acs.org/10.1021/acs.langmuir.3c00688

Notes

The authors declare no competing financial interest.

ACKNOWLEDGMENTS

This work was supported by the National Science Foundation through the University of California San Diego Materials Research Science and Engineering Center (UCSD MRSEC), grant number DMR-2011924. This work was performed in part at the San Diego Nanotechnology Infrastructure (SDNI) of University of California San Diego, a member of the National Nanotechnology Coordinated Infrastructure (NNCI), which was supported by the National Science Foundation (Grant ECCS-1542148). Electron microscopy images were taken in the Cellular and Molecular Medicine Electron microscopy core facility, which was supported in part by the National Institutes of Health Award number S10OD023527. This work was supported in part through CHE-2116298, which funded the stipend and tuition for Z.W.

■ REFERENCES

- (1) Khan, M. R.; Adam, V.; Rizvi, T. F.; Zhang, B.; Ahamad, F.; Jośko, I.; Zhu, Y.; Yang, M.; Mao, C. Nanoparticle-Plant Interactions: A Two-Way Traffic. *Small* **2019**, *15* (37), No. e1901794.
- (2) Chen, H.; Shao, L.; Li, Q.; Wang, J. Gold Nanorods and Their Plasmonic Properties. *Chem. Soc. Rev.* **2013**, 42 (7), 2679–2724.
- (3) Yang, D.-P.; Cui, D.-X. Advances and Prospects of Gold Nanorods. Chemistry An Asian Journal 2008, 3 (12), 2010–2022.
- (4) Marinakos, S. M.; Chen, S.; Chilkoti, A. Plasmonic Detection of a Model Analyte in Serum by a Gold Nanorod Sensor. *Anal. Chem.* **2007**, 79 (14), 5278–5283.
- (5) Dickerson, E. B.; Dreaden, E. C.; Huang, X.; El-Sayed, I. H.; Chu, H.; Pushpanketh, S.; McDonald, J. F.; El-Sayed, M. A. Gold Nanorod Assisted Near-Infrared Plasmonic Photothermal Therapy (PPTT) of Squamous Cell Carcinoma in Mice. *Cancer Letters* **2008**, 269 (1), 57–66.
- (6) Tang, H.; Xu, X.; Chen, Y.; Xin, H.; Wan, T.; Li, B.; Pan, H.; Li, D.; Ping, Y. Reprogramming the Tumor Microenvironment through Second-Near-Infrared-Window Photothermal Genome Editing of PD-L1Mediated by Supramolecular Gold Nanorods for Enhanced Cancer Immunotherapy. *Adv. Mater.* **2021**, *33* (12), No. 2006003.

- (7) Wang, C.; Chen, Y.; Wang, T.; Ma, Z.; Su, Z. Monodispersed Gold Nanorod-Embedded Silica Particles as Novel Raman Labels for Biosensing. *Adv. Funct. Mater.* **2008**, *18* (2), 355–361.
- (8) Hu, L.; Li, Y.; Peng, X.; Zheng, W.; Xu, W.; Zhu, J.; Lee, L. Y. S.; Chu, P. K.; Wong, K.-Y. TiO2 Film Supported by Vertically Aligned Gold Nanorod Superlattice Array for Enhanced Photocatalytic Hydrogen Evolution. *Chem. Eng. J.* **2021**, *417*, No. 127900.
- (9) Milikić, J.; Stamenović, U.; Vodnik, V.; Ahrenkiel, S. P.; Šljukić, B. Gold Nanorod-Polyaniline Composites: Synthesis and Evaluation as Anode Electrocatalysts for Direct Borohydride Fuel Cells. *Electrochim. Acta* 2019, 328, No. 135115.
- (10) Kim, J.-U.; Cha, S.-H.; Shin, K.; Jho, J. Y.; Lee, J.-C. Synthesis of Gold Nanoparticles from Gold(I)—Alkanethiolate Complexes with Supramolecular Structures through Electron Beam Irradiation in TEM. J. Am. Chem. Soc. 2005, 127 (28), 9962–9963.
- (11) Brust, M.; Walker, M.; Bethell, D.; Schiffrin, D. J.; Whyman, R. Synthesis of Thiol-Derivatised Gold Nanoparticles in a Two-Phase Liquid–Liquid System. *J. Chem. Soc., Chem. Commun.* **1994**, 0 (7), 801–802.
- (12) Yu, Y.; Yan, L.; Si, J.; Xu, Y.; Hou, X. Femtosecond Laser Assisted Synthesis of Gold Nanorod and Graphene Hybrids and Its Photothermal Property in the Near-Infrared Region. *J. Phys. Chem. Solids* **2019**, *132*, 116–120.
- (13) Losic, D.; Shapter, J. G.; Mitchell, J. G.; Voelcker, N. H. Fabrication of Gold Nanorod Arrays by Templating from Porous Alumina. *Nanotechnology* **2005**, *16* (10), 2275.
- (14) Jégat, C.; Rollin, E.; Douillard, L.; Soppera, O.; Nakatani, K.; Laurent, G. Patterning Gold Nanorod Assemblies by Deep-UV Lithography. J. Phys. Chem. C 2022, 126 (32), 13729–13738.
- (15) Bittner, A. M.; Alonso, J. M.; Górzny, MŁ.; Wege, C. Nanoscale Science and Technology with Plant Viruses and Bacteriophages. In Structure and Physics of Viruses: An Integrated Textbook; Mateu, M. G., Ed.; Subcellular Biochemistry; Springer Netherlands: Dordrecht, 2013; pp 667–702.
- (16) Koudelka, K. J.; Pitek, A. S.; Manchester, M.; Steinmetz, N. F. Virus-Based Nanoparticles as Versatile Nanomachines. *Annual Review of Virology* **2015**, 2 (1), 379–401.
- (17) Han, L.; Shao, C.; Liang, B.; Liu, A. Genetically Engineered Phage-Templated MnO2 Nanowires: Synthesis and Their Application in Electrochemical Glucose Biosensor Operated at Neutral PH Condition. ACS Appl. Mater. Interfaces 2016, 8 (22), 13768–13776.
- (18) Santhoshkumar, J.; Rajeshkumar, S.; Venkat Kumar, S. Phyto-Assisted Synthesis, Characterization and Applications of Gold Nanoparticles A Review. *Biochem. Biophys. Rep.* **2017**, *11*, 46–57.
- (19) Ahmad, T.; Iqbal, J.; Bustam, M. A.; Irfan, M.; Anwaar Asghar, H. M. A Critical Review on Phytosynthesis of Gold Nanoparticles: Issues, Challenges and Future Perspectives. *J. Cleaner Prod.* **2021**, 309, No. 127460.
- (20) Wong, M. H.; Giraldo, J. P.; Kwak, S.-Y.; Koman, V. B.; Sinclair, R.; Lew, T. T. S.; Bisker, G.; Liu, P.; Strano, M. S. Nitroaromatic Detection and Infrared Communication from Wild-Type Plants Using Plant Nanobionics. *Nat. Mater.* **2017**, *16* (2), 264–272.
- (21) Shukla, S.; Marks, I.; Church, D.; Chan, S.-K.; K Pokorski, J.; F Steinmetz, N. Tobacco Mosaic Virus for the Targeted Delivery of Drugs to Cells Expressing Prostate-Specific Membrane Antigen. *RSC Adv.* **2021**, *11* (33), 20101–20108.
- (22) Lim, J.-S.; Kim, S.-M.; Lee, S.-Y.; Stach, E. A.; Culver, J. N.; Harris, M. T. Quantitative Study of Au(III) and Pd(II) Ion Biosorption on Genetically Engineered Tobacco Mosaic Virus. *J. Colloid Interface Sci.* **2010**, 342 (2), 455–461.
- (23) Geiger, F. C.; Eber, F. J.; Eiben, S.; Mueller, A.; Jeske, H.; Spatz, J. P.; Wege, C. TMV Nanorods with Programmed Longitudinal Domains of Differently Addressable Coat Proteins. *Nanoscale* **2013**, *5* (9), 3808–3816.
- (24) Huang, Y.; Chiang, C.-Y.; Lee, S. K.; Gao, Y.; Hu, E. L.; Yoreo, J. D.; Belcher, A. M. Programmable Assembly of Nanoarchitectures Using Genetically Engineered Viruses. *Nano Lett.* **2005**, *5* (7), 1429–1434.

- (25) QCM-DlMeasurements/Biolin Scientific. https://www.biolinscientific.com/measurements/qcm-d#what-is-qcm-d. (accessed 2023-01-30).
- (26) Höök, F.; Kasemo, B.; Nylander, T.; Fant, C.; Sott, K.; Elwing, H. Variations in Coupled Water, Viscoelastic Properties, and Film Thickness of a Mefp-1 Protein Film during Adsorption and Cross-Linking: A Quartz Crystal Microbalance with Dissipation Monitoring, Ellipsometry, and Surface Plasmon Resonance Study. *Anal. Chem.* **2001**, 73 (24), 5796–5804.
- (27) Steinmetz, N. F.; Findlay, K. C.; Noel, T. R.; Parker, R.; Lomonossoff, G. P.; Evans, D. J. Layer-By-Layer Assembly of Viral Nanoparticles and Polyelectrolytes: The Film Architecture Is Different for Spheres Versus Rods. *ChemBioChem.* **2008**, 9 (10), 1662–1670.
- (28) Love, A. J.; et al. The use of tobacco mosaic virus and cowpea mosaic virus for the production of novel metal nanomaterials. *Virology* **2014**, *449*, 133–139.
- (29) Knez, M.; Sumser, M.; Bittner, A. M.; Wege, C.; Jeske, H.; Martin, T. P.; Kern, K. Spatially Selective Nucleation of Metal Clusters on the Tobacco Mosaic Virus. *Adv. Funct. Mater.* **2004**, *14* (2), 116–124.
- (30) Reimers, J. R.; Ford, M. J.; Halder, A.; Ulstrup, J.; Hush, N. S. Gold Surfaces and Nanoparticles Are Protected by Au(0)—Thiyl Species and Are Destroyed When Au(I)—Thiolates Form. *Proc. Natl. Acad. Sci. U.S.A.* **2016**, *113* (11), E1424—E1433.
- (31) Radloff, C.; Vaia, R. A.; Brunton, J.; Bouwer, G. T.; Ward, V. K. Metal nanoshell assembly on a virus bioscaffold. *Nano Lett.* **2005**, *5* (6), 1187–1191.
- (32) Nourbakhsh, M. S.; Khosroshahi, M. E. An In-Vitro Investigation of Skin Tissue Soldering Using Gold Nanoshells and Diode Laser. *Lasers Med. Sci.* **2011**, 26 (1), 49–55.
- (33) Oliveira, J. P.; Prado, A. R.; Keijok, W. J.; Ribeiro, M. R. N.; Pontes, M. J.; Nogueira, B. V.; Guimarães, M. C. C. A Helpful Method for Controlled Synthesis of Monodisperse Gold Nanoparticles through Response Surface Modeling. *Arabian J. Chem.* **2020**, 13 (1), 216–226.
- (34) Jalil, S. U.; Zahera, M.; Khan, M. S.; Ansari, M. I. Biochemical Synthesis of Gold Nanoparticles from Leaf Protein of Nicotiana Tabacum L. Cv. Xanthi and Their Physiological, Developmental, and ROS Scavenging Responses on Tobacco Plant under Stress Conditions. *IET Nanobiotechnol.* **2019**, *13* (1), 23–29.
- (35) Yu, G.; Vago, F.; Zhang, D.; Snyder, J. E.; Yan, R.; Zhang, C.; Benjamin, C.; Jiang, X.; Kuhn, R. J.; Serwer, P.; Thompson, D. H.; Jiang, W. Single-Step Antibody-Based Affinity Cryo-Electron Microscopy for Imaging and Structural Analysis of Macromolecular Assemblies. *J. Struct. Biol.* **2014**, *187* (1), 1–9.